



TITLE:

Oxide particle coarsening at temperature over 1473 K in 9CrODS steel

AUTHOR(S):

Oono, N.; Nakamura, K.; Ukai, S.; Kaito, T.;
Torimaru, T.; Kimura, A.; Hayashi, S.

CITATION:

Oono, N. ...[et al]. Oxide particle coarsening at temperature over 1473 K in 9CrODS steel. Nuclear Materials and Energy 2016, 9: 342-345

ISSUE DATE:

2016-12

URL:

<http://hdl.handle.net/2433/218605>

RIGHT:

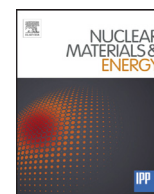
© 2016 The Authors. Published by Elsevier Ltd. This is an open access article under the CC BY-NC-ND license (<http://creativecommons.org/licenses/by-nc-nd/4.0/>).



Contents lists available at ScienceDirect

Nuclear Materials and Energy

journal homepage: www.elsevier.com/locate/nme



Oxide particle coarsening at temperature over 1473 K in 9CrODS steel



N. Oono^{a,*}, K. Nakamura^a, S. Ukai^a, T. Kaito^b, T. Torimaru^c, A. Kimura^d, S. Hayashi^e

^a Hokkaido University, Faculty of Engineering, Materials Science, N13, W8, Kita-ku, Sapporo 060-8628, Japan

^b Japan Atomic Energy Agency, 4002 Narita, O-arai, Ibaraki 311-1393, Japan

^c Nippon Nuclear Fuel Development Co., Ltd. 2163 Narita, O-arai, Ibaraki 311-1393, Japan

^d IAE, Kyoto University, Gokasho, Uji, Kyoto 611-0011, Japan 0.3

^e Tokyo Institute of Technology, 2-12-1, Ookayama, Meguro-ku Tokyo 152-8550, Japan

ARTICLE INFO

Article history:

Available online 5 July 2016

ABSTRACT

The oxide particle coarsening was evaluated at temperature over 1473 K by means of transmission electron microscopy (TEM). After annealing of the 9CrODS extruded bar, the size of oxide particles increases while the number density decreases, indicating that the oxide particles coarsen through Ostwald ripening. The growth rate of the oxide particles follows the fifth-power law, which is in the region of dislocation ‘pipe’ diffusion. The activation energy for pipe diffusion, however, was remarkably high, derived as 891 kJ/mole. The stability of oxide particles and the difference of the diffusion velocity in between bcc- δ phase and fcc- γ phase should be considered as the contributions to the activation energy.

© 2016 The Authors. Published by Elsevier Ltd.

This is an open access article under the CC BY-NC-ND license

(<http://creativecommons.org/licenses/by-nc-nd/4.0/>).

1. Introduction

9CrODS steel is known as the advanced structural material for the future fusion blanket system, because of its high-temperature strength and superior radiation resistance due to finely dispersed oxide particle [1–4]. 9CrODS steel usually contains a small amount of Ti, which reduces the size of oxide particles and thereby significantly improves the creep strength [1]. The concept of the addition of Ti is adopted not only for 9CrODS steel, but also for other ODS ferritic steels [5, 6]. The oxide particles in the Ti-added ODS ferritic steels are very stable even at high temperature, even above 1273 K [7–11]. This stability is due to the low interfacial energy of Y–Ti complex oxide [12]. However, as for 9CrODS steel, the orientation relationship between Y–Ti complex oxide and matrix should be changed at above 1173 K because of the phase transformation from bcc- α to fcc- γ [13]. This work is based on a fundamental study about the kinetics of coarsening of oxide particles in 9CrODS steel at high temperature. In this work, systematic high temperature annealing was done on 9CrODS steel to observe and estimate the mechanism of coarsening of oxide particles.

2. Experimental procedure

An extruded bar of 9CrODS steel, whose chemical composition is 9Cr-0.13C-2W-0.2Ti-0.35Y₂O₃ (in mass%), was cut into several

pieces (we call them “as-received” pieces). The pieces were annealed in a vacuum furnace at a vacuum $\sim 1 \times 10^{-4}$ Torr, in order to coarsen oxide particles. The annealing temperatures and time are listed in Table 1. The temperature increase and decrease rate was 5 K/min. The as-received and annealed pieces were punched into 3mm ϕ disc specimens and electro-polished. Transmission electron microscope (TEM) images were taken from the as-received specimen and annealed specimens to measure the oxide particle size distribution and number density, at using JEOL JEM-2010 operated at 200 kV. We analyzed the mean size by a direct measurement of the oxide particles. In order to calculate number density, the thickness of the specimen was measured by convergent-beam electron diffraction (CBED). The thickness ranges from 70 nm to 181 nm.

3. Results and discussion

Fig. 1 shows TEM micrographs of oxide particles before and after high temperature annealing. After annealing at 1623 K for 27 h, oxide particles become more than three times larger than those of as-received. Fig. 2 shows the size distribution of oxide particles before and after annealing. The peak of the size is increase with increasing annealing temperature. The distribution does not appear to be bimodal. The average size and number density of oxide particles after annealing are plotted in Fig. 3(a) and (b), respectively. The average size increases with increase in both annealing temperature and time. On the contrary, the number density decreases with an increase in the average size of oxide particles, which indicates that the oxide particles coarsen through Ostwald ripening.

* Corresponding author. Fax: +81117066356.

E-mail address: n-oono@eng.hokudai.ac.jp (N. Oono).

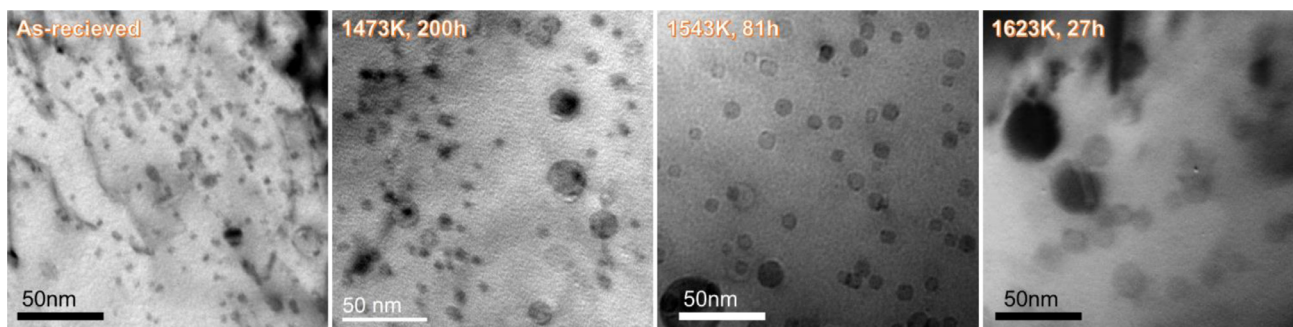


Fig. 1. TEM image of oxide particles in 9CrODS steel (as-received, 1473 K 200 h, 1543 K 81 h, 1623 K 27 h).

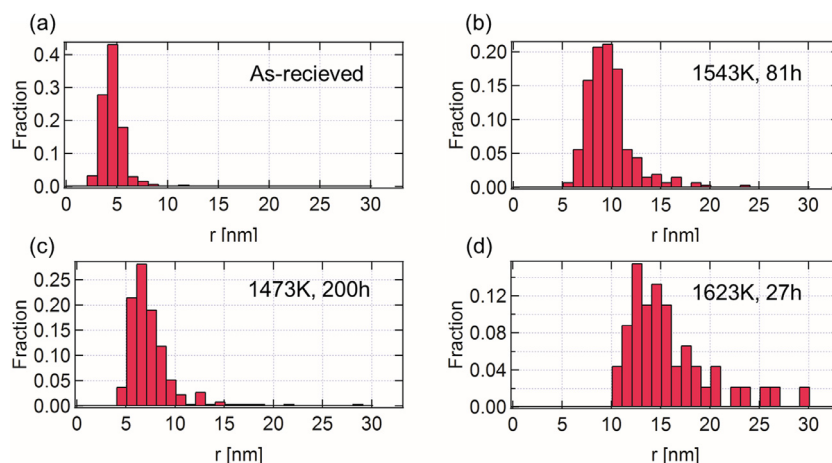


Fig. 2. Size distribution of the oxide particles: (a) as-received, (b) 1473 K, 200 h, (c) 1543 K, 81 h, (d) 1623 K, 27 h.

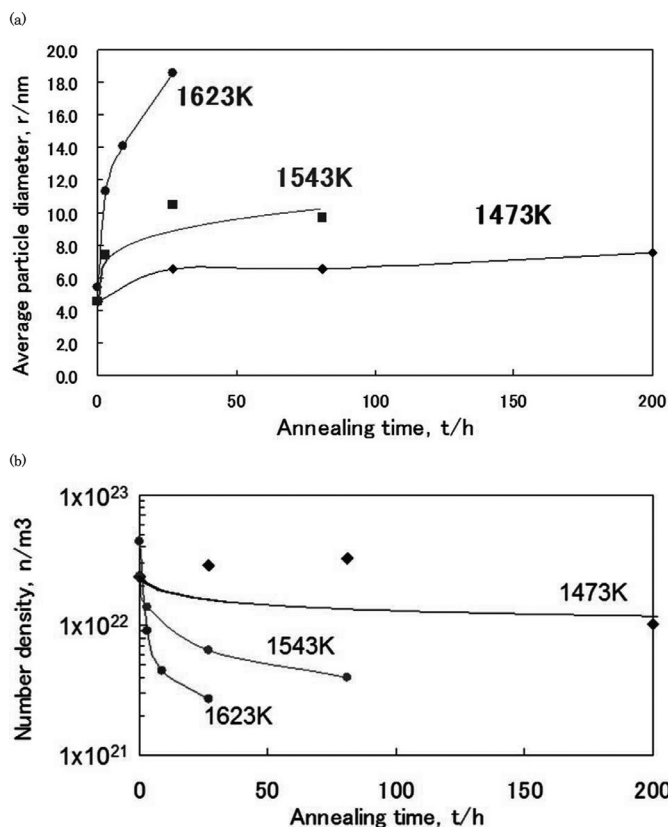


Fig. 3. (a) Average size and (b) Number density of oxide particles in 9CrODS steel after annealing.

Table 1

Annealing conditions for 9CrODS steel pieces.

Temperature [K]	Time [h]		
1473	27	81	200
1543	3	27	81
1623	3	9	27

Table 2

Slopes of $\ln(r^n - r_0^n)$ versus $\ln(t)$ for the values of n : $n = 3$, 4 and 5 at each annealing temperature.

Temperature [K]	$n = 3$	$n = 4$	$n = 5$
1473	0.31	0.37	0.43
1543	0.33	0.41	0.49
1623	0.70	0.92	1.14

Given the kinetic relationship for precipitate coarsening through Ostwald ripening [14]:

$$r^n - r_0^n = k \cdot \exp(-Q/RT) \cdot t \quad (1)$$

where r and r_0 is precipitate radius after and before annealing, respectively, k is the rate constant for a specific temperature and diffusive process, t is the annealing time, and the exponent n is the value restricted by the mechanisms of diffusion: $n = 3$ for lattice diffusion, $n = 4$ for grain-boundary diffusion and $n = 5$ for dislocation 'pipe' diffusion [14]. Taking logarithm for Eq. (1), it gives:

$$\ln(r^n - r_0^n) = A + \ln(t) \quad (2)$$

where $A = -(Q/RT) \cdot \ln(k)$, is a constant at given temperature. Fig. 4 and Table 2 show a corresponding plot of $\ln(r^n - r_0^n)$ versus $\ln(t)$ for variable n at 1623 K and the values of the slope of the line fits at all annealing temperatures, respectively. At 1623 K,

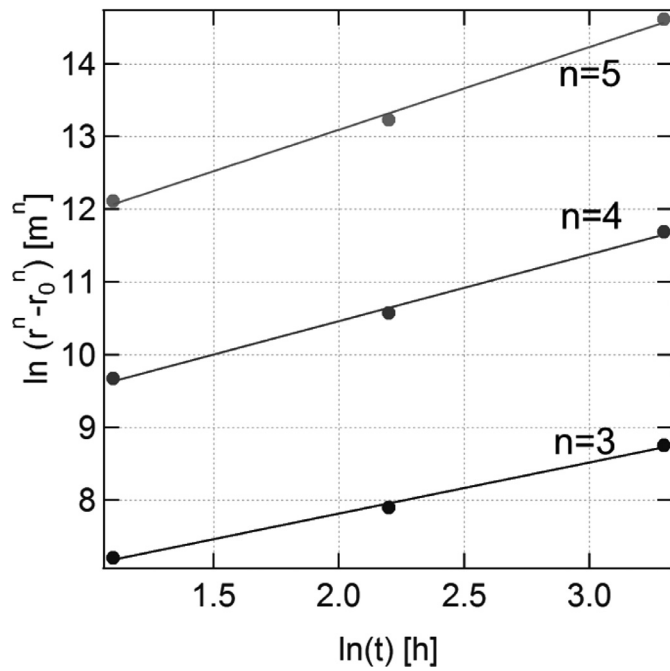


Fig. 4. Corresponding plot of $\ln(r^n - r_0^n)$ versus $\ln(t)$ for variable n at 1623 K.

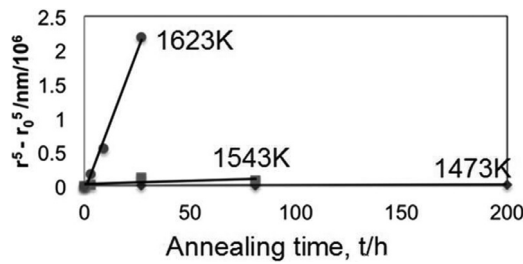


Fig. 5. Plot of t versus $r^5 - r_0^5$ applying $n = 5$ to Eq. (3).

the slope for $n = 4$ should be adopted. However, at lower temperatures, 1473 K and 1543 K, the slope for $n = 5$ is much closer to 1 than that of $n = 4$. It is difficult to judge which n is suitable considering the slope at lower temperatures. In this paper, we prefer the mean value of the slope of 1473 K, 1543 K and 1623 K to calculate the diffusion activation energy (Q). We choose $n = 5$, which corresponds to a pipe diffusion mechanism.

The Eq. (1) can be rewritten as the following equations:

$$r^n - r_0^n = B \cdot t \quad (3)$$

$$B = k \cdot \exp(-Q/RT) \quad (4)$$

Taking logarithm for Eq. (4):

$$\ln(B) = -Q/RT + \ln(k) = -Q/R \cdot (1/T) + \ln(k) \quad (5)$$

Applying $n = 5$ to Eq. (3), t versus $r^5 - r_0^5$ curve can be plotted as shown in Fig. 5. The value of B in the Eqs. (3) and (4) can be obtained by the fit to the data $r^5 - r_0^5$ and t in Fig. 5. Fig. 6 shows the corresponding fit to the $\ln(B)$ versus $1/T$ with the values of B obtained by the fits in Fig. 5. The slope of the fit in Fig. 6 yields a diffusion activation energy Q of 891 kJ/mol and k of 2.78×10^{33} /s.

The value of Q obtained in the present work is remarkably higher than that of the yttrium diffusion in iron (approximately 200 kJ/mole) [15]. Some other contributions affecting to the value should be considered. One of the contributions is the stability of oxide particles. For example, the standard Gibbs free energy

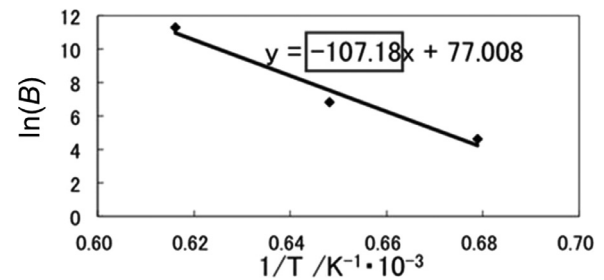


Fig. 6. Plot of $\ln(B)$ versus $1/T$ with the values of B obtained by the fits in Fig. 5.

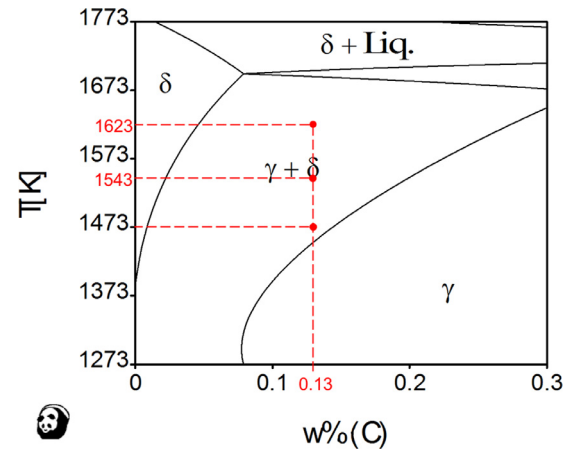


Fig. 7. Phase diagram of 9CrODS steel; black circles indicate experimental condition.

of formation of Y_2O_3 is very large (-960 kJ/mole) [16], and solubility of yttrium and oxygen in ferrite matrix is very low (less than 1%) [17]. Another contribution is matrix transformation at high temperature. Fig. 7 shows a phase diagram of 9CrODS steel calculated by using a commercial software [18]. The matrix at a temperature above 1473 K contains fcc- γ and bcc- δ dual phases. The molar fraction of the δ phase increase from 0.06 to 0.56 with increase in temperature from 1473 K to 1623 K [18]. For example, the pre-exponential factor and the diffusion activation energy of self-diffusion in α -iron are higher than those of γ -iron [19] and the expressions for diffusion coefficient of α -iron and δ -iron are completely same [20]. Considering the ratios of lattice and grain-boundary self-diffusion in α -iron and γ -iron, $D_v(\alpha)/D_v(\gamma) = 110$ and $D_{gb}\delta(\alpha)/D_{gb}\delta(\gamma) = 7$ [19], and the ratio of the δ phase as described above, the present ratios of self-diffusion $D_v(1623K)/D_v(1473K)$ and $D_{gb}\delta(1623K)/D_{gb}\delta(1473K)$ will be calculated as follows:

$$\begin{aligned} D_v(1623K)/D_v(1473K) &= (D_v(\alpha) * 0.56 + D_v(\gamma) * (1 - 0.56)) / (D_v(\alpha) * 0.06 \\ &\quad + D_v(\gamma) * (1 - 0.06)) \\ &= (110D_v(\gamma) * 0.56 + D_v(\gamma) * (1 - 0.56)) / (110D_v(\gamma) * 0.06 \\ &\quad + D_v(\gamma) * (1 - 0.06)) \\ &\cong 8.23 \end{aligned} \quad (6)$$

$$\begin{aligned} D_{gb}\delta(1623K)/D_{gb}\delta(1473K) &= (D_{gb}\delta(\alpha) * 0.56 + D_{gb}\delta(\gamma) * (1 - 0.56)) / \\ &\quad (D_{gb}\delta(\alpha) * 0.06 + D_{gb}\delta(\gamma) * (1 - 0.06)) \\ &= (7D_{gb}\delta(\gamma) * 0.56 + D_{gb}\delta(\gamma) * (1 - 0.56)) / \\ &\quad (7D_{gb}\delta(\gamma) * 0.06 + D_{gb}\delta(\gamma) * (1 - 0.06)) \\ &\cong 3.21 \end{aligned} \quad (7)$$

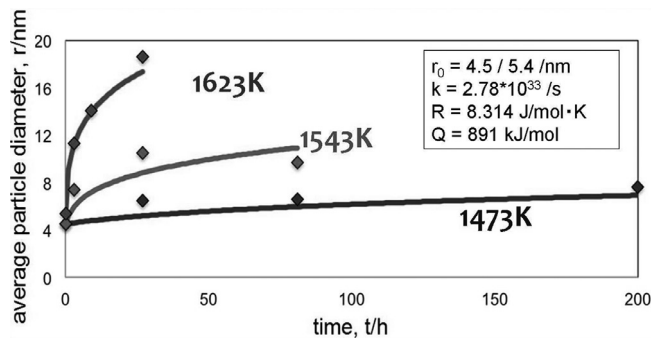


Fig. 8. Overlaying the estimation curve with the graph shown in Fig. 2.

Although there is no data of yttrium and oxygen short-circuit diffusion in γ - and δ -iron, the tendency of the diffusion probably follows that of the self-diffusion in iron. The increase in the ratio of the δ phase can lead a large value of Q , because the diffusion of the elements in bcc- δ phase is usually accelerated than that in fcc- γ phase.

The radius of oxide particles after annealing can be estimated from the deformed equation of (1):

$$r = [k \cdot \exp(-Q/RT) \cdot t + r_0^5]^5 \quad (8)$$

The value of r corresponding to a certain annealing temperature (T) and time (t) can be estimated by assigning the constant values k , Q and r_0 for the Eq. (8), where Q is 891 kJ/mol, k is $2.78 \times 10^{33}/s$ (calculated from Eq. (5) and Fig. 6). Fig. 8 shows the overlaying of plot of r versus t in Fig. 3(a), with the estimated values of r and t . The estimation curves agree with the experimental values.

4. Conclusion

Coarsening of oxide particles in 9CrODS steel at high temperature above 1473 K was studied by annealing of the specimens. The size of oxide particles increases while the number density decreases, indicating that the oxide particles coarsen through Ostwald ripening. The coarsening data is consistent with a pipe diffusion mechanism. The fit of the data yields the remarkably high activation energy of diffusion, 891 kJ/mole, indicating that other

contributions, such as the stability of oxide particles, should be considered. The estimation curves agree with the experimental values.

Acknowledgements

This study is the result of “R&D of ODS ferritic steel fuel cladding for maintaining fuel integrity at the high temperature accident condition” entrusted to Hokkaido University by the Ministry of Education, Culture, Sports, Science and Technology of Japan (MEXT).

References

- [1] S. Ohtsuka, S. Ukai, M. Fujiwara, T. Kaito, T. Narita, J. Nucl. Mater. 329–333 (2004) 372–376.
- [2] H. Sakasegawa, S. Ohtsuka, S. Ukai, H. Tanigawa, M. Fujiwara, H. Ogiwara, et al., Fus. Eng. Des. 81 (2006) 1013–1018.
- [3] A.G. Certain, K.G. Field, T.R. Allen, M.K. Miller, J. Bentley, J.T. Busby, J. Nucl. Mater. 407 (2010) 2.
- [4] A. Certain, S. Kuchibhatla, V. Shutthanandan, D.T. Hoelzer, T.R. Allen, J. Nucl. Mater. 434 (2013) 311–321.
- [5] S. Ukai, M. Fujiwara, J. Nucl. Mater. 307–311 (2002) 749–757.
- [6] I.-S. Kim, B.-Y. Choi, C.-Y. Kang, T. Okuda, P.J. Maziasz, K. Miyahara, ISIJ Int. 43 (2003) 1640–1646.
- [7] M.K. Miller, D.T. Hoelzer, E.A. Kenik, K.F. Russell, J. Nucl. Mater. 329–333 (2004) 338–341.
- [8] M.K. Miller, D.T. Hoelzer, E.A. Kenik, K.F. Russell, Intermetallics 13 (2005) 387–392.
- [9] Y. Ortega, V. de Castro, M.A. Monge, A. Muñoz, T. Leguey, R. Pareja, J. Nucl. Mater. 376 (2008) 222–228.
- [10] H. Sakasegawa, F. Legendre, L. Boulanger, M. Brocq, L. Chaffron, T. Cozzika, J. Malaplate, J. Henry, J. Nucl. Mater. 417 (2011) 229–232.
- [11] S.Y. Zhong, J. Ribis, V. Klosek, Y. de Carlan, N. Lochet, V. Ji, M.H. Mathon, Y. de Carlan, J. Nucl. Mater. 428 (2012) 154–159.
- [12] J. Ribis, M.-L. Lescoat, S.Y. Zhong, M.-H. Mathon, Y. de Carlan, J. Nucl. Mater. 442 (2013) S101–S105.
- [13] M. Yamamoto, S. Ukai, S. Hayashi, T. Kaito, S. Ohtsuka, J. Nucl. Mater. 417 (2011) 237–240.
- [14] M.J. Alinger, On The Formation And Stability Of Nanometer Scale Precipitates In Ferritic Alloys During Processing And High Temperature Service PhD Thesis, University of California Santa Barbara, California, 2004.
- [15] D. Murali, B.K. Panigrahi, M.C. Valsakumar, C.S. Sundar, J. Nucl. Mater. 419 (2011) 208–212.
- [16] Y. Awakura, S. Banya, et al., Physical Chemistry Of Metals, The Japan Institute of Metals, 1996.
- [17] B. Thaddeus, Massalski H. Okamoto, P.R. Subramanian, L. Kacprzak, Binary Alloy Phase Diagrams, 2, Second Edition, ASM International, 1990.
- [18] M. Yamamoto, S. Ukai, S. Hayashi, T. Kaito, S. Ohtsuka, Mater. Sci. and Eng. A 527 (2010) 4418–4423.
- [19] D.W. James, G.M. Leak, Phil. Mag. 12 (1965) 491–503.
- [20] D.W. James, G.M. Leak, Phil. Mag. 14 (1966) 701–713.